Theoretical Study of p-i-n Photodetectors' Power Limitations from 2.5 to 60 GHz

Joseph Harari, Guanghai Jin, Jean P. Vilcot, and Didier Decoster

***Abstract*—In this paper, we present a theoretical study and a numerical simulation of various long wavelength top-illuminated p-i-n photodetectors in the frequency range of 2.5–60 GHz under high optical modulated power at 1.55-μm wavelength. The modeling includes a monodimensional Drift–Diffusion model for the device and takes into account the external circuit. We considered six InP/GaInAs/InP photodetectors especially designed to work at 2.5, 10, 20, 30, 40, and 60 GHz, respectively. For the one with the highest frequency, we intentionally sacrificed the quantum efficiency in order to compare them at the end with the results already obtained in the case of waveguide p-i-n photodetectors. The results show the maximum microwave-output power for each photodetector at its specific working frequency. Additionally, we present the effects of the modulation depth, the back illumination, and the wavelength 1.3 μm.**

***Index Terms*— Numerical analysis, optical interconnections, photodectors, p-i-n photodiodes, power transmission.**

I. Introduction

FOR high microwave-power distribution, optical links can be an interesting solution because of the physical insulation, small size, and weak attenuation of optical fibers in the long wavelength domain. Over the last few years, numerous research have been carried out in this field. The improvements of the link particularly concerned cutoff frequency and maximum optical power delivered by photodetectors [1]–[4]. The behavior of p-i-n photodetectors under high optical modulated power has been studied theoretically as well as experimentally [5]–[12]. The research we have already presented dealt with a top-illuminated p-i-n photodiode at 20 GHz [13], and also with a waveguide p-i-n photodetector at 60 GHz [14]. In previous papers, we precisely identified the different parameters which influence the behavior of the photodetector under high optical power. Among these parameters, the spot size is very important, as is the photodiode illuminated volume. All of theses results motivated us to continue our study with the same modeling tool, taking into consideration various top-illuminated p-i-n photodiodes in the frequency range of 2.5–60 GHz.

II. Simulated P-I-N Photodiodes and Models

The simulated photodetectors are classical p+ InP/n− GaInAs/n+ InP heterostructures whose doping levels are $10^{18}/10^{15}/10^{18}$ cm^{-3}, respectively. The p+/n− junction is located at the InP/GaInAs heterointerface. As is well known, the small signal-cutoff frequency of such a device is governed by two different effects: the carrier transit time in the depleted region of the photodetector and the influence of photodiode capacitance in the external circuit. For cutoff frequencies lower than 25 GHz, the transit time limitation makes the use of a sufficiently thick (1.5-μm) GaInAs absorbing layer possible, which results in high quantum efficiency. However, for higher cutoff frequencies, the transit time limitation necessitates the decrease of the undoped layer thickness, which reduces the quantum efficiency. Moreover, if the undoped layer thickness is thinner, the photodetector surface has to be reduced in order to decrease the device capacitance. These rules drove us to successively choose six device structures (GaInAs n− thickness, photodiode surface) in order to get a microwave-output signal at 2.5, 10, 20, 30, 40, and 60 GHz. For the highest frequencies, we intentionally decrease the GaInAs thickness and thus, the photodiode quantum efficiency. All characteristics of the simulated photodiodes are presented in Table I.

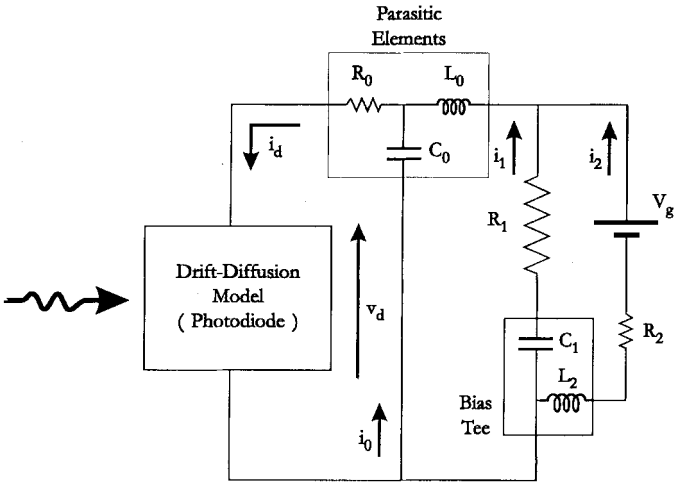

Fig. 1. Whole circuit introduced in the numerical simulation.

In our study, the modeling tool already used in our previous literature [13], [14], is composed of a complete monodimensional Drift–Diffusion model with the equations introducing the external circuit which is composed of the resistor (R_2) of the dc generator, the components (C_1, L_2) of the bias tee, the microwave load (R_1), and the parasitic elements (R_0, C_0, L_0), as represented in Fig. 1.

III. Results and Analysis

A. Behavior Under High Modulated Optical Power

The different phenomena which reduce the photodiode dynamic-response efficiency under high modulated optical

Manuscript received June 12, 1996; revised April 10, 1997.

The authors are with the Institut d'Electronique et de Microélectronique du Nord, UMR CNSR, 59652 Villeneuve d'Ascq Cedex, France.

Publisher Item Identifier S 0018-9480(97)05991-7.

TABLE I
SIMULATED PHOTODIODE STRUCTURES WITH THEIR SMALL-SIGNAL CHARACTERISTICS AT 1.55-μM WAVELENGTH AND THE ELEMENTS OF THE EXTERNAL CIRCUIT ESPECIALLY CHOSEN TO STUDY THE PHOTODETECTOR BEHAVIOR AT THE MODULATION FREQUENCY

Photodiode	**1**	**2**	**3**	**4**	**5**	**6**
Modulation Frequency (GHz)	2.5	10	20	30	40	60
GaInAs Thickness (μm)	2.5	2.5	1.5	0.8	0.6	0.4
Simulated Thickness (μm)	3	3	2	1.3	1.1	0.9
Diameter (μm)	140	60	22	20	15	10
Cut-off frequency (GHz)	4.3	11.6	21.6	34	46.7	67.3
Quantum efficiency	0.82	0.82	0.64	0.42	0.33	0.24
Bias voltage (V)	9	9	5	2.2	1.4	0.6
C_1 (nF)	0.8	0.2	0.1	0.066	0.05	0.033
L_2 (μH)	20	5	2.5	1.67	1.25	0.83
R_0 (Ω)	-	5	-	-	5	-
C_0 (fF)	-	10	-	-	10	-
L_0 (nH)	-	0.5	-	-	0.01	-

power are the carrier effect in the photodetector and the modification of the instantaneous photodiode bias voltage due to high photocurrent in the external circuit.

For a high input optical signal, the carrier densities increase in the photodetector depleted zone and become higher than the InGaAs-layer doping level. This specific carrier distribution leads to a sharp decrease of the electric field near the n−/n+ heterointerface. This phenomenon is cumulative since it reduces the carrier velocity and thus, increase the carrier densities. This is shown in Fig. 2, which depicts the electric field in structure two at 10 GHz under 500-mW optical modulated power (modulation depth equal to 1). In these conditions, structure two, which has a large surface, forces the appearance of the carrier effect and the external circuit. Curve *b* of Fig. 2 is the electric field when the instantaneous photocurrent is minimum. The photodetector is not fast enough to maintain an electrical modulation depth equal to 1, and thus, the photocurrent is not equal to zero. The external circuit then leads to the increase of the photodiode bias voltage. As a consequence, the electric field becomes very high near the p+/n− heterointerface. Half a period (50 ps) later, the photocurrent is maximum, which decreases the bias voltage, and the carrier distribution changes, as does the electric field (curve *c*). The hole and electron densities are very high and almost the same near the n−/n+ interface. In this region, since the electric field is never equal to zero (see the inset of Fig. 2), the carriers have some built-in velocity. These characteristics allow us to consider that this region behaves like a doped neutral region. Moreover, the zone of the high electric-field region near the junction is approximately 0.9-μm thick, and this thickness changes slightly with the instantaneous output photocurrent. For all these reasons, we can consider that the

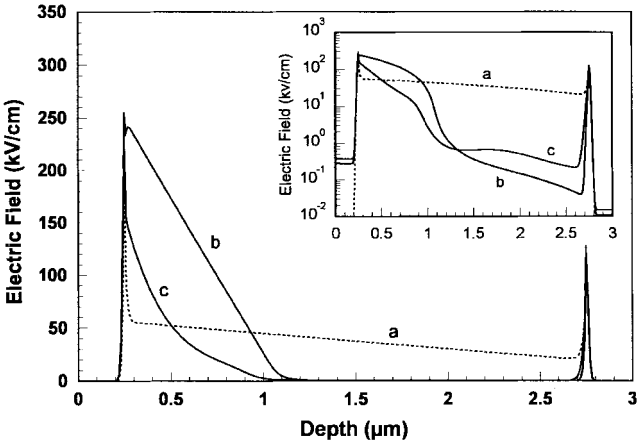

Fig. 2. Electric field in structure 2 at 10 GHz for an optical power of 500 mW with a modulation depth equal to 1. *a* under small-signal *b* at a minimum of photocurrent *c* at a maximum photocurrent. (logarithmic Y scale in inset).

effective photodiode capacitance increases. Obviously, this phenomenon depends on the photodiode structure, the external circuit, and the optical power distribution in the photodetector.

B. Parasitic Effects Due to Very High Electric Field

It is well known that a band-to-band tunneling effect occurs in the n− GaInAs at high electric fields [17], [18]. The exact critical field value, which particularly depends on the material growth conditions, is difficult to calculate. However, the studies that have already been done in order to optimize avalanche photodiode structures [18], [19] demonstrate that we can start from a critical value around 250 kV/cm. In our case, such an electric field is reached and even exceeded at the

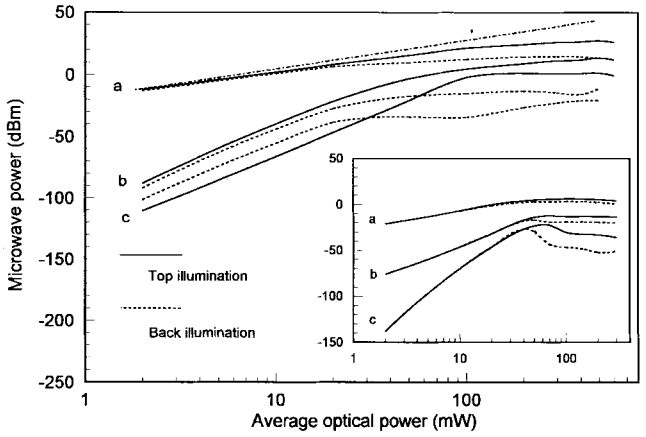

Fig. 3. Microwave response of structure 2 at 10 GHz under top and bottom illumination. The modulation depth is 100%. a is fundamental, while b and c are harmonics of order two and three. The straight line represents a constant responsivity. Insert: Similar response of structure 5 at 40 GHz.

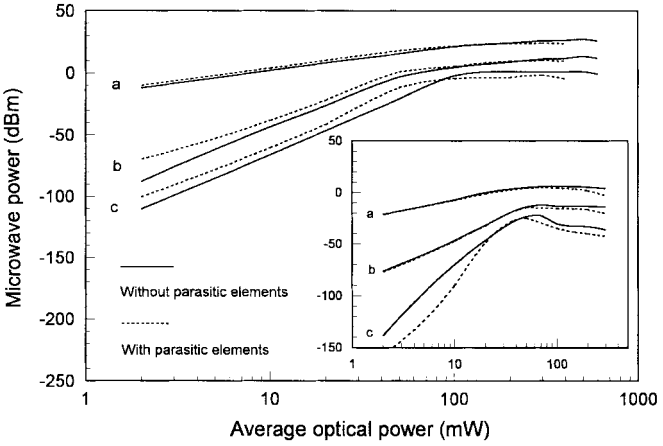

Fig. 4. Microwave response of structure 2 at 10 GHz and influence of the parasitic elements. The modulation depth is 100%. a is fundamental, while b and c are harmonics of order two and three. Insert: Similar response of structure 5 at 40 GHz.

p+/n− heterojunction when the optical power increases. For some optical powers, it is reached periodically only for certain times when the photocurrent is high and the depolarization is not too high. But for higher optical powers, the electric-field average value at the heterojunction exceeds 250 kV/cm [13]. The only thing we know in such a condition is that a parasitic tunneling current occurs and can cause the device breakdown. Thus, we consider that this situation is not satisfying for the device reliability and must be avoided. For all presented results, the heterojunction electric field is not too high when the output power saturation occurs, but increases dangerously with more increasing optical power, and as consequence, the saturation effectively gives the limit of the photodetector behavior.

C. Influence of the Wavelength and Bottom Illumination

For thin photodiodes (i.e., structure 5), as well as for thick photodiodes (i.e., structure 1), our calculations demonstrated little difference between the microwave responses at 1.55 and 1.3 μm. For small optical power, the fundamental level is a little bit higher at 1.55 μm than at 1.3 μm due to slightly higher responsivity at the higher wavelength. Even for very high optical powers, the difference between the fundamentals at 1.3 and 1.55 μm does not exceed 1 dB (those at 1.3 μm are higher). For the harmonic levels, this difference does not exceed 4 dB, and generally, a similar evolution versus average optical power does occur. In all photodiodes studied so far, the behavior at 1.3- and 1.55-μm wavelength is nearly same. As a consequence, we think that all results presented in the following sections at 1.55-μm wavelength can be used to estimate the distortion and saturation effects at 1.3 μm.

We then simulated bottom illumination for structures 2 and 5 at 10 and 40 GHz, respectively. The microwave responses obtained for top (p+ side) and bottom (n+ side) illuminations are presented in Fig. 3 and its inset, respectively. In both cases, the bottom illumination leads to a decrease of the output microwave power for the high optical-input signal, and also to a decrease of the harmonic levels compared to the fundamental one. The fact that this phenomenon is more pronounced for structure 2 than for structure 5 demonstrates the importance of the absorbing-layer thickness. In the case of top illumination, the generation rate is the highest near the p+/n− heterointerface; thus, among the carriers which take part in the electrical signal, the majority of hole–electron pairs are generated near the p+ layer and the average hole transit path is small, while those of electrons are long. Because of the higher electron velocity compared to the first hole, the device is faster than it is for back illumination. In this last case, the situation is opposite and the hole transit path becomes very long. For thin structures, the difference between these two illumination schemes is smaller, and one can expect less difference in output power, which can be seen by comparing Fig. 3 and its inset.

D. Influence of the Parasitic Elements

Fig. 4 demonstrates that the influence of the parasitic elements on the behavior under a high optical signal is weak at 10 GHz as well as at 40 GHz. These elements behave as a second-order filter for the microwave-output signal, and their effect is, in principle, independent of the microwave-output power. However, in the simulated circuit, the modification of the photodiode bias voltage is due to the modulated part $R_1 i_1$ and to the dc part $R_2 i_2$. In saturation conditions, the dc part of the photocurrent is very high, so its influence directly depends on the dc generator's internal resistance. In these conditions, the photodiode depolarization is increased by the specific contact resistance from the value $R_0 i_d \# R_0(i_1+i_2)$ if we assume that the effect of C_0 is weak. Thus, the contact resistance R_0 leads to a decrease of the maximum microwave-output power of a few decibels. Furthermore, because the photocurrent passing through the photodiode is very high, each parasitic resistance will particularly introduce power dissipation and possibly thermal physico–chemical instabilities in the device.

E. Full Results Concerning the Six Simulated Photodiodes from 2.5 to 60 GHz

In order to illustrate the precise importance of the illuminated photodiode absorbing volume, we first considered the

TABLE II
RESPONSIVITY OF THE SIX SIMULATED PHOTODIODES UNDER SATURATION CONDITION. P_{opt} IS THE OPTICAL POWER AT SATURATION, R_0 IS THE RESPONSIVITY IN SMALL-SIGNAL CONDITION (IN A/W), R_p IS THE ONE UNDER VERY HIGH OPTICAL INPUT POWER, AND H1/H3 IS THE RATIO OF FUNDAMENTAL COMPARED TO ORDER 3 HARMONIC AT SATURATION

Photodiode	**1**	**2**	**3**	**4**	**5**	**6**
Frequency (GHz)	2.5	10	20	30	40	60
P_{opt} (mW)	800	500	250	160	130	100
R_p/R_0	0.32	0.29	0.26	0.23	0.21	0.18
H1/H3 (dB)	16.4	28.2	34.1	35.7	36.6	36.8

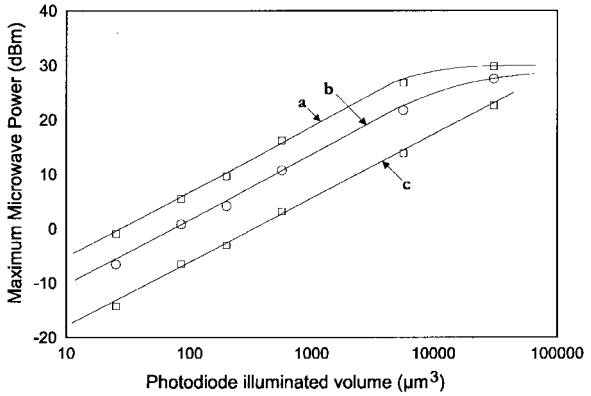

Fig. 5. Maximum microwave-output power versus photodiode illuminated volume for different modulation depth m. a denotes $m = 1$, b denotes $m = 0.5$, and c denotes $m = 0.2$. This curve has been obtained for the six photodiodes of Table I.

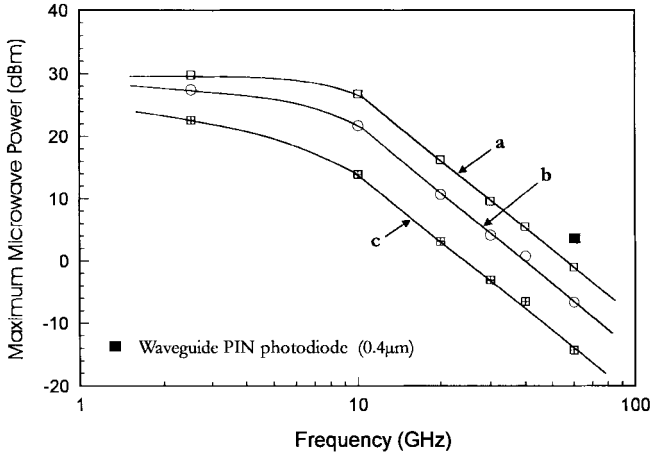

Fig. 6. Maximum microwave-output power versus modulation frequency for different modulation depth m. a denotes $m = 1$, b denotes $m = 0.5$, and c denotes $m = 0.2$. This curve has been obtained for the six photodiodes of Table I.

maximum microwave-output power of the six photodiodes versus their illuminated volume (Fig. 5) and we simulated the case of three different modulation depths: $m = 1$, $m = 0.5$, and $m = 0.2$. For a given modulation depth, the maximum output power is directly proportional to the photodiode illuminated volume. Exception to this law exists only for big volumes where the photocurrent is sufficiently high in the external circuit to cause a sharp decrease of the photodetector bias voltage, which enhances the carrier effect. Moreover, the greater the modulation depth, the more the maximum microwave-output power is because the saturation effect is mainly dependent on the carrier density in the depleted zone of the photodiode; thus, for a higher dc part of the photocurrent, a stronger limitation effect takes place. For these results, we only considered the saturation of the output modulated photocurrent, where the heterojunction electric field is not critical. Fig. 5 can be completed by Fig. 6, showing the maximum microwave-output power versus modulation frequency. As already explained in the Section II, this last curve considered that for a given frequency the photodiode volume is as big as possible. In these conditions, there is a tradeoff between frequency and power, as already described, for example, in the case of transistors. The significant photodetector characteristics have been resumed as shown in Table II, for each photodiode with the average optical power where saturation occurs, the value of responsivity at saturation compared to the small signal responsivity, and the third harmonic level compared to the fundamental one at saturation. Furthermore, all curves presented show that the saturation point is close to the 1-dB compression point (difference of 3 dB). As a consequence, Figs. 5 and 6 are valuable to know, from a general point of view, the limitations in these conditions.

To compare with the performances of waveguide p-i-n photodetectors, we set the point representing the performance of the 0.4-μm-thick side-illuminated multimode photodiode studied in [14], as shown in Fig. 6. For this photodetector, the spot width is 4 μm and the device length is 12 μm. The waveguide photodiode performance is some decibels higher than structure 6 at 60 GHz due to completely different light distribution in the absorbing layer and also to the better responsivity of the side-illuminated photodetector compared to those of structure 6.

IV. CONCLUSION

We presented the modeling of microwave p-i-n photodetectors under high optical power based on a monodimensional Drift–Diffusion model and taking into account the external circuit. The simulated photodiodes are classical top-illuminated InP/GaInAs/InP heterostructures with a cutoff frequency between 2.5 and 60 GHz. Our results demonstrated the weak influence of the wavelength on the behavior under a high modulated signal, and the great influence of bottom illumination mainly in the case of a photodiode with a thick absorbing layer

(2.5 μm). The influence of parasitic elements has been studied at 10 and 40 GHz, and shows the importance of the parasitic resistance due to the photodiode ohmic contact and the external connection system. We then presented the combined evolution of maximum microwave-output power and photodiode illuminated volume, and as a consequence, the linear decrease of the maximum output power with increased modulation frequency. A comparison with the results already obtained for p-i-n waveguide photodiodes at 60 GHz has then been carried out and the different characteristics of all photodiodes simulated under saturation conditions have been presented. The microwave power which can be obtained from such photodiodes is some tens of decibels, but the nonlinearities in these conditions are important. Because the illumination conditions are of great importance, it would be interesting to make a study under a high optical signal of evanescent coupling-wave photodetectors or to consider traveling-wave photodetectors.

REFERENCES

[1] J. Schlafer, C. B. Su, W. Powazinik, and R. B. Lauer, "20 GHz bandwidth InGaAs photodetector for long wavelength microwave optical links," *Electron. Lett.*, vol. 21, no. 11, pp. 469–471, 1985.

[2] K. Kato and J. Yoshida, "Ultrawide bandwidth 1.55 μm waveguide PIN photodiode," *Proc. SPIE–Int. Soc. Opt. Eng.*, vol. 2149, pp. 312–319, Jan. 1994.

[3] A. R. Williams, A. L. Kellner, A. L. Jiang, and P. K. L. Yu, "InGaAs/InP waveguide photodetector with high saturation intensity," *Electron. Lett.*, vol. 28, no. 24, pp. 2258–2259, 1992.

[4] I. S. Ashour, J. Harari, J. P. Vilcot, and D. Decoster, "High optical power nonlinear dynamic response of AlInAs/GaInAs MSM photodiode," *IEEE Trans. Electron. Devices*, vol. 42, pp. 828–834, May 1995.

[5] M. Dentan and B. de Cremoux, "Numerical simulation of the nonlinear response of a PIN photodiode under high illumination," *J. Lightwave Technol.*, vol. 8, pp. 1137–1144, Aug. 1990.

[6] R. D. Esman and K. J. Williams, "Measurement of harmonic distortion in microwave photodetectors," *IEEE Photon. Technol. Lett.*, vol. 2, pp. 502–504, July 1990.

[7] K. J. Williams and R. D. Esman, "Observation of photodetector nonlinearities," *Electron. Lett.*, vol. 28, no. 8, pp. 731–733, 1992.

[8] R. R. Hayes and D. L. Persechini, "Nonlinearity of PIN photodetectors," *IEEE Photon. Techol. Lett.*, vol. 5, pp. 70–72, Jan. 1993.

[9] K. J. Williams, R. D. Esman, and M. Dagenais, "Effect of high space-charge fields on the response of microwave photodetectors," *IEEE Photon. Technol. Lett.*, vol. 6, pp. 639–641, May 1994.

[10] K. J. Williams, "Nonlinear mechanisms in microwave photodetectors operated with high intrinsic region electric fields," *Appl. Phys. Lett.*, vol. 65, no. 10, pp. 1219–1221, 1992.

[11] A. R. Williams, A. L. Kellner, and P. K. L. Yu, "High frequency saturation measurements of an InGaAs/InP waveguide photodetector," *Electron. Lett.*, vol. 29, no. 14, pp. 1298–1299, 1993.

[12] D. Wake, N. G. Walker, and I. C. Smith, "Zero-bias edge coupled InGaAs photodiodes in millimeter wave radio fiber systems," *Electron. Lett.*, vol. 29, no. 21, pp. 1879–1881, 1993.

[13] J. Harari, G. Jin, F. Journet, J. Vandecasteele, J. P. Vilcot, C. Dalle, M. R. Friscourt, and D. Decoster, "Modeling of microwave top illuminated PIN photodetector under very high optical power," *IEEE Trans. Microwave Theory Tech.*, vol. 44, pp. 1484–1487, Aug. 1996.

[14] J. Harari, F. Journet, O. Rabii, G. Jin, J. P. Vilcot, and D. Decoster, "Modeling of waveguide PIN photodetectors under very high optical power," *IEEE Trans. Microwave Theory Tech.*, vol. 43, pp. 2304–2310, Sept. 1995.

[15] D. Hahn, O. Jaschinski, H. H. Wehmann, and A. Schlachetzki, "Electron concentration dependence of absorption and refraction in N− InGaAs near the band edge," *J. Electron. Mater.*, vol. 24, no. 10, pp. 1357–1361, 1995.

[16] K. Kato, S. Hata, K. Kawano, J. Yoshida, and A. Kozen, "A high efficiency 50 GHz InGaAs multimode waveguide photodetector," *IEEE J. Quantum. Electron.*, vol. 28, pp. 2728–2735, Dec. 1992.

[17] S. R. Forrest, M. Didomenico, R. G. Smith, and H. J. Stocker, "Evidence for tunneling in reverse-biased III–V photodetector diodes," *Appl. Phys. Lett.*, vol. 36, no. 7, pp. 580–582, 1980.

[18] H. Ando, H. Kanbe, M. Ito, and T. Kaneda, "Tunneling current in InGaAs and optimum design for InGaAs/InP avalanche photodiodes," *Jpn. J. Appl. Phys.*, vol. 19, no. 6, pp. 277–280, 1980.

[19] J. Harari, D. Decoster, J. P. Vilcot, B. Kramer, C. Oguey, P. Salzac, and G. Ripoche, "Numerical simulation of avalanche photodiodes with guard ring," *Proc. Inst. Elect. Eng.*, vol. 138, pt. J, pp. 211–217, June 1991.

Joseph Harari was born in Enghien, France, in 1961. He received the engineer degree from the Polytechnic Institute of Grenoble, Grenoble, France, in 1985, and the Ph.D. degree from the University of Lille, Lille, France, in 1991.

In 1992, he joined the Institut d'Electronique et de Microélectronique du Nord, Département Hyperfréquences et Semiconducteurs. He is currently an Assistant Professor at the Engineering School, University of Lille (Ecole Universitaire d'Ingénieurs de Lille, EUDIL). His current activities focus on the simulation and conception of optoelectronic devices for millimeter-wave applications, integrated optics devices, and optical interconnection.

Guanghai Jin was born in Harbin, China, in 1960. He received the B.S. and M.S. degrees in applied physics from Harbin Institute of Technology, Harbin, China, in 1982 and 1984, respectively. In 1994, he joined the Institut d'Electronique et de Microélectronique du Nord, Villeneuve d'Ascq Cedex, France, to work toward the Ph.D. degree.

From 1984 to 1994, he worked as an Assistant Professor at Harbin Institute of Technology. His research activities include the study of integrated optics on $LiNbO_3$. His primary interests are on integrated optoelectronic devices and integrated optics.

Jean Pierre Vilcot was born in Lens, France, in 1958. He received the Ph.D. degree in electronics from the University of Lille, Lille, France in 1984.

From 1984 to 1986, he worked as a Microwave Engineer, mainly in the field of X-band satellite receivers. In 1986, he joined the Centre Hyperfrequence et Semiconducteurs (now Institut d'Electronique et de Microélectronique du Nord, Département Hyperfréquences et Semiconducteurs), Villeneuve d'Ascq Cedex, France, as a Scientist for the Centre National de la Recherche Scientifique (CNRS). His current activities include photonic and optoelectronic integrated circuits, microwave-optical interactions and optical interconnection.

Didier Decoster was born in Lille, France, in 1948. He received the Ph.D. degree in electronics and physical science (Doctorat d'Etat) from the University of Lille, Lille, France, in 1981.

He is currently a Professor in the Material Science Department, Engineering School of the University of Lille (Ecole Universitaire d'Ingénieurs de Lille, EUDIL). His research activities are with the Institut d'Electronique et de Microélectronique du Nord (IEMN), where he is the leader for the electromagnetism, optoelectronics and opto-acoustics group. His own activities include optoelectronic and photonic components and integrated circuits on III–V materials, microwave applications of optics, and optical interconnection.